Article

High-Speed Laser Drying of Lithium-Ion Battery Anodes: Challenges and Opportunities

Samuel Fink [1],*[iD], Delil Demir [1][iD], Markus Börner [2][iD], Vinzenz Göken [2] and Christian Vedder [1]

[1] Fraunhofer Institute for Laser Technology ILT, Steinbachstraße 15, 52074 Aachen, Germany; delil.demir@ilt.fraunhofer.de (D.D.); christian.vedder@ilt.fraunhofer.de (C.V.)
[2] MEET Battery Research Center, University of Muenster, Corrensstraße 46, 48149 Muenster, Germany; markus.boerner@uni-muenster.de (M.B.); vinzenz.goeken@uni-muenster.de (V.G.)
* Correspondence: samuel.fink@ilt.fraunhofer.de; Tel.: +49-241-8906-624

Abstract: In modern electrode manufacturing for lithium-ion batteries, the drying of the electrode pastes consumes a considerable amount of space and energy. To increase the efficiency of the drying process and reduce the footprint of the drying equipment, a laser-based drying process is investigated. Evaporation rates of up to 318 $\mathrm{g\ m^{-2}\ s^{-1}}$ can be measured, which is orders of magnitude higher than the evaporation rates in conventional furnace drying processes. Optical measurements of the slurry components in the visible and near-infrared spectrum are conducted. Thermal analyses the of laser-dried samples reveal that the commonly used binders carboxymethyl-cellulose (CMC) and styrene–butadiene rubber (SBR) are not affected by the laser drying process within the investigated process window. The results indicated that with the combination of a fast laser drying step and a subsequent convection drying step, high evaporation rates can be achieved while maintaining the integrity and adhesion of the anode.

Keywords: laser drying; lithium-ion batteries; optical characterization; binder degradation; photonic processing

1. Introduction

The challenge of climate change, which we are currently facing, demands the exploitation of renewable energy sources and the development of energy-storing technologies. Lithium-ion batteries (LIBs) are currently the most frequently used energy storage system in portable consumer electronics and e-mobility, with more applications still in development. Due to their high energy and power densities, LIBs have a high potential for applications in which weight and performance are key. First introduced by Sony in 1990 [1], LIBs have been improved in terms of performance, safety, recycling, and processing technology. The increasing demand for LIBs requires the further development of processing technologies. Despite increasing productivity to serve the growing market, geopolitical changes in recent years require increasing the efficiency and reducing the energy consumption of the manufacturing process.

One of the most energy-intensive steps in LIB production is electrode manufacturing. This process consists of mixing the materials, usually a water-based graphite slurry with polymeric binders, coating this anode slurry on copper foil, drying the anode and a calendaring step. Drying, meaning the removal of the water from the anode slurry, requires a large amount of energy. Considering processing speeds of the anode foil of 100 m/min or more, this drying process requires large furnaces, which take up a lot of space in production facilities. Both factors present significant cost drivers in LIB production.

This issue has led to the development of technologies that can reduce the energy consumption and the footprint of the drying units. In recent years, alternative drying technologies have been investigated to allow for higher web speeds, smaller footprints of the drying units and reduced energy consumption.

Infrared (IR) dryers are considered one alternative. In contrast to conventional convection drying, the energy is transferred to the wet slurry via radiation, which can reduce heat losses in the manufacturing equipment (like drying module walls, coils, etc.). Based on a computational approach introduced by Oppegård et al. that describes drying based on radiation, the drying time can be reduced [2]. Wu et al. have also compared infrared drying and convection drying when using a cathode material [3]. Their results indicate that, when used in the right drying stage, drying time and energy consumption can be reduced by using infrared drying. The parameters with the largest impact on the results were identified as emitter power and the distance between the emitter and the electrode. However, both groups state that air velocity and air temperature in an IR drying process can influence the drying speed and evaporation rates.

In parallel to IR drying, laser-based drying approaches have been investigated by Vedder et al., who were able to show that energy consumption can be reduced by 50% compared to a conventional furnace drying process [4].

According to Horsting et al., photonic drying technologies (IR drying and laser drying) have been developed in the recent years to a technology readiness levels (TRLs) of 8 and 7, respectively [4,5]. Both technologies can provide high evaporation rates but exhibit drawbacks concerning the penetration depth of the radiation into the slurry and the tendency to form defects in the anode. In this article, the limits of a fast laser drying process of water-based anode slurries are examined.

The laser drying process is schematically depicted in Figure 1. The laser radiation is transformed into thermal energy when it is absorbed by the components of the wet slurry. With a high-volume fraction and a high absorbance, graphite particles, as well as conductive carbon, are mainly responsible for the absorption of the laser radiation by the anode slurry. The increase in temperature leads to the evaporation of the volatile solvent, in this case water, until the anode is dry. During this process, the water content, as well as the thickness of the coating, decreases. The drying process can be divided into several steps, which have been described in detail by several authors [6–8]. In accordance with these findings, the most important steps are the consolidation of the film accompanied by the shrinking of the film and the emptying of the pores. These steps can differ depending on the evaporation rate, the energy transfer within the film and particle transport (e.g., binder migration). According to Jaiser et al., high drying rates enhance binder migration, which reduces the adhesion between the anode and the current collector [9]. This reduction negatively impacts the performance of the battery and can even lead to the delamination of the anode. In conventional convection drying, rates between 0.01 and 15 $g\,m^{-2}\,s^{-1}$ have been investigated by Kumberg et al. [8]. They were able to show that with increasing evaporation rate, the adhesion force between the anode and the current collector foil is drastically reduced, and cracks begin to occur at evaporation rates above 6 $g\,m^{-2}\,s^{-1}$.

What sets a laser-based drying process apart from conventional convection drying using hot air or IR drying is the high energy input in a short amount of time. This can lead to temperature gradients within the anode. as depicted in Figure 1, and thus, to differences in the drying states between the top and bottom layer of the anode. One important parameter that can have a large impact on the laser-based drying process is, for example, the optical penetration depth of the laser radiation into the wet slurry. The deeper the light can penetrate, the more homogeneous the wet slurry will heat up, which can prevent temperature-gradient-induced defects, like cracks or bubble formation.
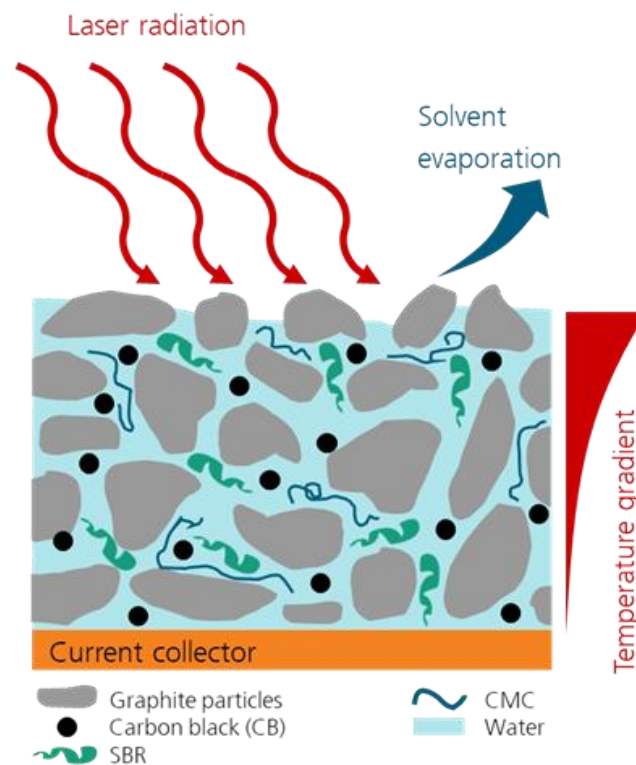
Figure 1. Schematic of the cross-section of a wet anode slurry during drying via irradiation with laser radiation.

Short interaction times between the laser and the slurry at high laser intensities can lead to the formation of local hotspots, for example, at the surface of the slurry. If the temperature exceeds the thermal stability threshold of the organic components, thermal degradation of these components can occur.

To gain detailed insights into the interaction between laser radiation and the components of the wet slurry, optical analysis methods are applied in this study to further increase the efficiency of the laser-based drying process while maintaining the properties and performance of the final product. The main objective of this article is to test the limits of evaporation rates in a laser drying process and compare them to conventional convection drying. The interaction between the laser beam and the different components of the slurry is investigated, and possible degradation processes of the organic components are examined. The results of this article can help in the development of laser-based drying equipment in large-scale battery production and provide an indication of the potential of fast anode drying.

2. Materials and Methods

2.1. Slurry Preparation and Coating

A standard water-based anode slurry is used for the laser drying experiments. The solid fraction of the slurry consists of 94% natural graphite (Merck Millipore, Burlington, VT, USA), 3% conductive carbon (Super C65T C-NERGY, Bruxelles, Belgium), 2% carboxy–methylcellulose (CMC binder, Sigma Aldrich, St. Louis, MO, USA) and 1% styrene–butadiene rubber (SBR, Zeon Europe GmbH, Düsseldorf, Germany). In this study, 60% deionized water was added to this solid fraction as a solvent. The slurry is mixed in a high-energy laboratory mixer (Eirich GmbH, Hardheim, Germany) for one hour. The slurry is then applied to a 15 μm thick copper foil (Cu58, Schlenk, Roth, Germany) with an automated doctor blade and a slit width of 150 μm, resulting in a dry film thickness of 60–70 μm. The final coating weights are recorded as being between 5.25 and 4.63 mg/cm^2.

2.2. Laser Drying

The laser drying experiments are conducted in a stationary setup to precisely control interaction time, laser power and air flow. A schematic of the experimental setup is depicted in Figure 2. A 6000 W laser system with a wavelength of 980 nm is used (LDM6000 Laserline, Mülheim-Kärlich, Germany) together with a focusing optic that provides a homogeneous 100×100 mm^2 spot at a working distance of 200 mm. This combination results in a maximum laser intensity of 60 W/cm^2. A pressurized air supply with an air knife, as well as a horizontal slit suction unit, provide a laminar gas flow. After laser drying, the remaining water in the electrode is removed with a moisture analyzer (MA X2 RADWAG, Radom, Poland) at 160 °C until the mass does not change anymore. The gas flow during laser drying is set to 40 L/min.
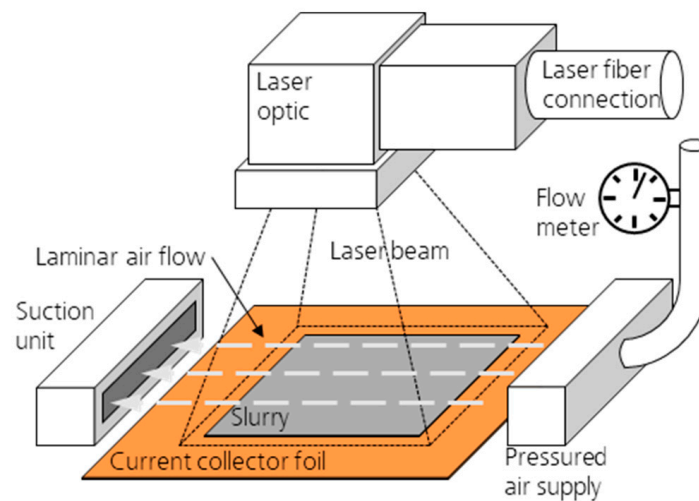
Figure 2. Schematic of the experimental setup for the laser drying experiments.

This combined process results in two separate drying regimes. The first section is defined by the laser parameters and the air flow. The second section, in which the remaining water is removed in the moisture analyzer (convection drying process), is defined by the drying temperature and the water vapor removal from the drying chamber, which is realized with an integrated fan. The resulting heating rates in the laser drying step might deviate drastically from the second drying step, where a constant temperature in the moisture analyzer is applied to remove the remaining water. The expected drying rates and water content are schematically depicted in Figure 3. From the weight difference between the points t1 and t2, the average drying rate in the laser drying step can be calculated. From the interaction time, the power, and the weight loss, the evaporation rate at a specific energy input is calculated. Due to the high intensities that can be reached in the laser drying process, the water content can be reduced at a higher rate than in a conventional convection drying process. The remaining water is then removed in a subsequent drying step. With this combination, low water contents can be achieved faster than in a convection drying process only. This approach raises the question of whether the partial fast laser drying step affects the properties (like adhesion reduction due to binder migration) of the electrode in an undesired way. Despite the combination of laser drying and convection drying, the samples will be labeled as "laser dried" hereafter.
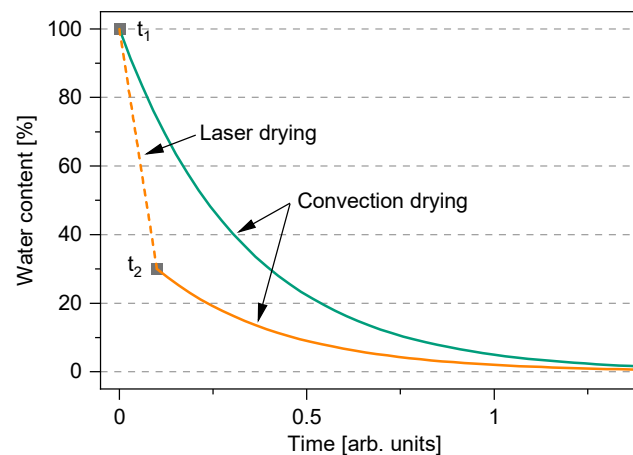
Figure 3. Schematic of the water content over time in a convection drying process (green) and a combined laser and convection drying process (orange). The time on the x-axis is chosen randomly and only schematically illustrates the difference between laser and convection drying.

2.3. Optical Characterization of Anode Components

The optical properties of the slurry components are analyzed in a spectrometer (UV-VIS-NIR spectrometer, Perkin Elmer, Waltham, MA, USA) for wavelengths between 350 and 2400 nm. An integrating sphere is used to ensure that scattered light is also collected and measured. The wet slurry components are placed between two microscopic slides that are set apart 140 µm with spacers. The reflection losses at the interfaces are considered and are removed from the absorption spectra accordingly. The transmittance T and reflectance R are measured, and the absorbance A is then calculated ($A = 100 - T - R$). For the copper foil and the dried anode on copper foil, only the reflectance is measured, as the transmittance equals zero. As only wet mixtures or dry electrodes can be measured, components like pure graphite, carbon black and solid CMC are not included in the measurement.

2.4. Thermographic Analysis (TGA)

TGA is carried out in a TGA Q5000 (TA Instruments, New Castle, DE, USA). The thermal stability of the samples was analyzed up to 600 °C for the laser-dried anodes. The TGA measurements are performed at a linear temperature ramp of 10 K min^{-1} under nitrogen gas flow. The measured parameter is the mass loss (weight) depending on the temperature.

2.5. Adhesion Testing

The adhesion tests are carried out on a tensile testing machine (Albrecht Zwick GmbH, Hagen, Germany). Double-coated urethane foam tape 4026 (3M, Saint Paul, MN, USA) is taped on two aluminum profiles with a defined area of 25×25 mm^2, which are installed into the tensile testing machine. The force is applied perpendicular to the anode surface. The samples are first compressed between the two aluminum profiles with a force of 20 N for 10 s to ensure adhesion of the tape. The adhesion test is then carried out until the anode detaches from the copper foil.

3. Results and Discussion

3.1. Optical Characterization of Anode Components

The absorption spectra of electrode components and mixtures of electrode components are presented in Figure 4. The dry and wet slurry both exhibit a high absorbance of over 90% within the measured spectral range. This high absorbance can be attributed to the graphite particles and the carbon black. The copper foil, used as the current collector, exhibits a low absorbance and high reflectance for wavelengths larger than 650 nm. Water and the water + CMC mixture (2% CMC in water) show similar results concerning the

absorbance. The characteristic absorption peaks at 1450 nm and 1935 nm can be attributed to water. The dissolved CMC does not seem to have a measurable impact on the optical properties of the slurry. The SBR dispersion also shows the characteristic water absorbance peaks, but compared to water, a larger absorbance can be measured for wavelengths below 1250 nm. This increased absorbance is attributed to light scattering and absorbance at the dispersed SBR particles.
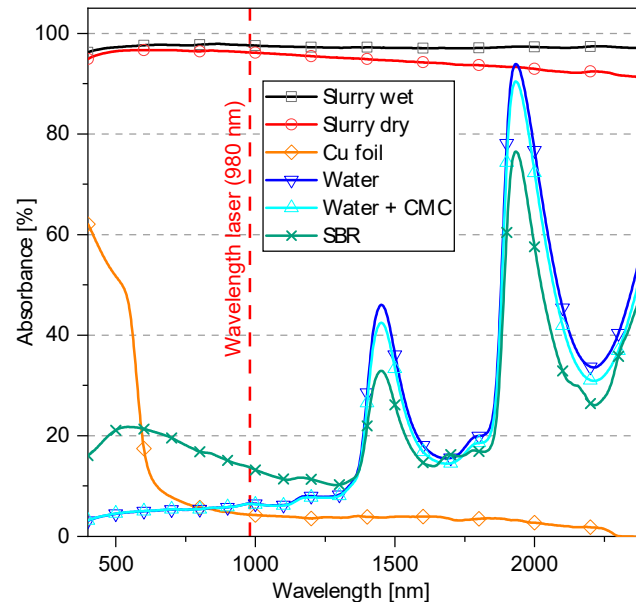

Figure 4. Absorbance for components in an LIB anode. The measurements are performed on 140 μm thick films (between two microscope slides) and a 65 μm thick film for the dry slurry, respectively. The wavelength of the laser used in the drying experiments is included in the graph.

The measurements show that the high absorbance of the graphite and the carbon black contributes to the high absorbance of the anode. For a laser-based drying approach, the high absorbance allows for an energetically efficient drying process, as most of the introduced photonic energy is transformed into heat. Assuming this process, the graphite particles on top will heat up first. The energy is then transferred into the surrounding water. From the binder system, only SBR might contribute to the absorbance of the slurry. Compared to the measured sample presented in Figure 4, the concentration of SBR in a conventional anode slurry is below 3% and thus will not affect the absorbance of the slurry significantly. Even if the SBR does not contribute to the cumulative absorbance of the slurry, the absorbance might be relevant in the laser-based drying process. In contrast to the CMC, laser radiation can directly interact with the SBR and might lead to thermal damages and even the decomposition of the SBR. As the optical penetration depth in the wet slurry is limited due to the high absorbance of the graphite particles, this damage might only occur on the surface of the electrode but could potentially impact the electrochemical performance of the cell. The thermal degradation of the SBR is investigated by means of TGA further below.

3.2. Results of Laser Drying Experiments

In the laser drying experiments, the interaction time and the laser power are varied in such a way that the energy input is kept constant at 7.2 J cm^{-2}. This value is derived from preliminary tests and proved to be suitable to allow for drying while limiting the formation of macroscopic defects like cracks or bubbles in the electrodes. The evaporation rate and the water loss in a laser-based drying process are presented in Figure 5. The measured water loss is constant at values between 40% and 45%, which is within the margin of error for all the power–interaction time combinations. The error is estimated via the drying of

multiple samples for one power–interaction time combination. The evaporation rate is calculated from the water loss and the interaction time. This leads to a linear relationship between the evaporation rate and power or interaction time, respectively, with a maximum evaporation rate of 318 g m^{-2} s^{-1} for a 6000 W laser power and 120 ms interaction time. Evaluation of the adhesion strength yields values between 27.2 and 30.7 N cm^2 without a systematic correlation between laser parameters and adhesion strength. Reference samples dried in a convection drying process exhibit adhesion strengths of 30 ± 1.5 N cm^{-2}, which shows that the laser drying process does not notably deteriorate the adhesion strength and leads to similar values within the margin of error determined for the reference sample. The laser-dried anodes all exhibit cracks, except for the one with the lowest evaporation rate of 63.7 g m^{-2} s^{-1}. The reference anodes, which are fully dried in the moisture analyzer at 160 °C, reach a level of water loss of 40 % after about 20 s. As the evaporation rate changes depending on the current water content, a reliable evaporation rate cannot be calculated.
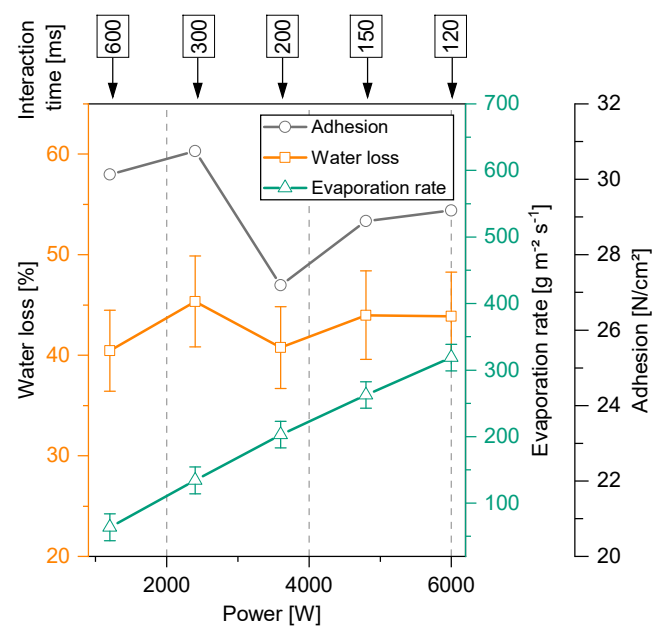

Figure 5. Water loss and evaporation rate for different power−interaction time combinations. The energy input is kept the same for all parameter sets at 7.2 J cm^{-2}.

The results indicate that the water loss is determined by the power put into the system and is, within the investigated process window, independent of variations in power and interaction time. On these timescales, energy losses due to radiation or heat conduction to the surroundings can be neglected. The evaporation rates that can be reached are an order of magnitude larger than those reported for other drying methods [8]. The measured adhesion strengths of the laser-dried anodes compared to the convection-dried reference indicate that binder migration is limited. As the sample is only partially dried after the laser drying process, presumably the binder is either not dislocated yet or has time to redistribute evenly in the anode before the final drying in the convection drying process.

3.3. Results of TGA Measurement

To verify the presumption that the binder is not affected by the laser drying process, TGA measurements are performed on selected laser-dried samples. The results are presented in Figure 6. The derivative of the mass loss dm/dT exhibits two pronounced decomposition regimes for all three samples. These reactions can be attributed to the thermal degradation of CMC (~250–320 °C) and SBR (~360–440 °C), respectively [10]. Two samples with short and long interaction times (120 and 600 ms) were analyzed. Compared to the reference that is convection-dried, no change in the position or intensity of the decomposition reactions can be observed. This means that during laser drying, neither CMC

nor SBR have experienced any kind of degradation due to the high laser intensities within the investigated parameter range. Considering the optical properties of both binders, SBR might be especially prone to premature degradation.
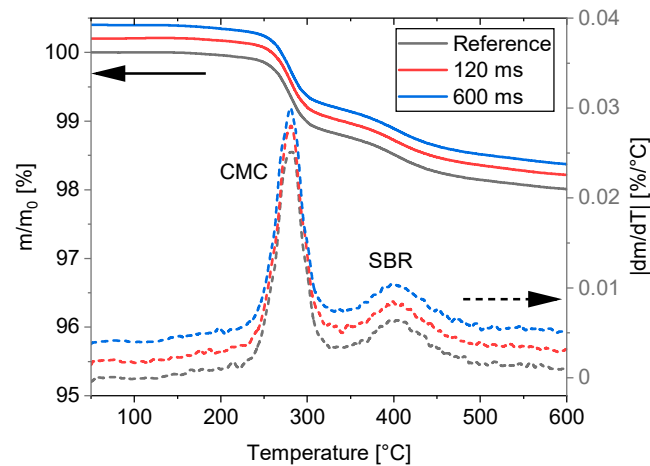
Figure 6. TGA results from selected samples. The derived curves of the parameters 120 and 600 ms in the graph are shifted by 0.002%/°C to make the overlying curves visible. The curves which depict the mass change are shifted by 0.2%. The peaks in the derived curves can be associated with the disintegration of CMC and SBR, respectively. The sold lines depict the relative mass change, the dashed lines depict the derivative of the relative mass change.

Despite the absorbance of the SBR in the anode (see Figure 4), the TGA measurements indicate no degradation of SBR. The SBR particles might accumulate on the surface of the graphite particle as they form a dispersion with the water. Assuming that the laser radiation is mainly absorbed by the graphite particles and converted into thermal energy, SBR particles on the graphite particle surface might experience high temperatures before being cooled down by the water. Either the concentration of SBR in the anode (3%) is too low to detect partial degradation, the temperature does not exceed a critical temperature, or the temperature is introduced on such a short timescale that degradation can be neglected. In the investigated samples, there is still water present in the anode after the laser drying step. Thus, a temperature that drastically exceeds the boiling point of water will only be reached locally within the graphite particles.

4. Conclusions

The increasing demand for energy storage capacities requires new and energy efficient manufacturing technologies for lithium-ion batteries. Laser-based drying offers a possible approach to increase the drying speed, decrease energy consumption, and provide an alternative to conventional gas-powered convection furnaces.

The optical properties of a typical LIB anode slurry are measured, and a stationary laser drying station is set up to investigate high evaporation rates. Drying experiments are conducted at a constant energy input of 7.2 J cm^{-2} while varying interaction time and laser power. The resulting evaporation rates are multiple orders of magnitude higher than the evaporation rates reached when using conventional furnace drying. Between 40% and 50% of the water in the slurry is removed during the laser drying, the remaining water is then removed in a subsequent conventional drying step. The laser-dried samples exhibit adhesion strength within the range of convection-dried reference anodes.

TGA measurements reveal that the binder components of CMC and SBR are not damaged by the laser radiation, overheating the temperature-sensitive components can thus be ruled out within the investigated parameter range. The laser-dried anodes exhibit cracks when interaction times below 600 ms are applied.

The presented results give an insight into the limits and potentials of a laser drying process. Extremely high evaporation rates can be achieved. However, the results point towards a combination process of laser drying for the first stage and convection drying for the second stage to achieve high evaporation rates while avoiding crack formation and delamination in the second stage. Another approach could be a distributed drying process, where multiple laser-drying modules are integrated into a continuous production process. This allows for an individual adjustment of the required energy input at different drying stages of the anode.

In future work, the impact of additional parameters like slurry composition, binder chemistry, film thickness and gas flow need to be investigated to be able to design a viable drying system that can be scaled for industrial applications. Another aspect that could be influenced by a fast drying process is the porosity of the anode. During the drying process, microscopic steam bubbles could form, which could lead to higher porosity in terms of the anode. Micro-computed tomography (micro-CT) can give an indication of the microstructure of the anode. As the porosity will be adjusted after the anode is fully dried in a calendering process, the effect of the laser drying on the performance needs to be investigated in functional cells.

The drying process can also be transferred to the cathode or other battery material systems like sodium-based battery designs. Considering the high heat capacity of water and the high enthalpy of evaporation, the removal of other solvents like NMP (N-Methyl-2-pyrrolidone) might even be more efficient and less energy-consuming. When considering the energy efficiency of a laser-based drying process, the limited conversion rate of the laser system must be considered. The current generation of diode lasers reach conversion efficiencies of up to 55 %. The remaining 45 % of thermal loss needs to be removed with an external cooling system. This makes the comparison between laser drying and conventional drying quite challenging. But due to the spatially and temporally dedicated energy input, laser drying shows a high potential in terms of being a competitive option. To properly compare the energy consumption of a conventional drying process with a laser-based system, a scale-up of the laser-based drying process to relevant web speeds is necessary. Stationary experiments can only help to gain insight into the basic processes relevant to a fast drying approach.

References

1. Kim, H.; Yoon, J.; Yoon, W.S. Polymorphic Consideration in Conversion Reaction-Based Anode Materials for Next-Generation Li Rechargeable Batteries. In *Electrochemical Society Meeting Abstracts*; The Electrochemical Society: Philadelphia, PA, USA, 2020; Volume 4, p. 544.
2. Oppegård, E.; Jinasena, A.; Strømman, A.H.; Suul, J.A.W.; Burheim, O.S. Study of an Industrial Electrode Dryer of a Lithium-Ion Battery Manufacturing Plant: Dynamic Modeling. In Proceedings of the SIMS 2020, Virtual, 22–24 September 2020; pp. 77–84.

3.   Wu, X.F.; Li, X.J.; Bei, X.Z. Experiments on Hot-Air and Infrared Drying Characteristics of LiCoO$_2$ Cathode Coating for Lithium-Ion Battery. *Mater. Sci. Forum* **2020**, *1003*, 260–267. [CrossRef]
4.   Vedder, C.; Hawelka, D.; Wolter, M.; Leiva, D.; Stollenwerk, J.; Wissenbach, K. Laser-based drying of battery electrode layers. In Proceedings of the ICALEO 35th International Congress on Applications of Lasers & Electro-Optics, San Diego, CA, USA, 16–20 October 2016; p. N501.
5.   von Horstig, M.W.; Schoo, A.; Loellhoeffel, T.; Mayer, J.K.; Kwade, A. A Perspective on Innovative Drying Methods for Energy-Efficient Solvent-Based Production of Lithium-Ion Battery Electrodes. *Energy Technol.* **2022**, *10*, 2200689. [CrossRef]
6.   Zhang, Y.S.; Courtier, N.E.; Zhang, Z.; Liu, K.; Bailey, J.J.; Boyce, A.M.; Richardson, G.; Shearing, P.R.; Kendrick, E.; Brett, D.J. A Review of Lithium-Ion Battery Electrode Drying: Mechanisms and Metrology. *Adv. Energy Mater.* **2022**, *2*, 2102233. [CrossRef]
7.   Westphal, B.; Bockholt, H.; Günther, T.; Haselrieder, W.; Kwade, A. Influence of Convective Drying Parameters on Electrode Performance and Physical Electrode Properties. *ECS Trans.* **2015**, *22*, 57–68. [CrossRef]
8.   Kumberg, J.; Bauer, W.; Schmatz, J.; Diehm, R.; Tönsmann, M.; Müller, M.; Ly, K.; Scharfer, P.; Schabel, W. Reduced Drying Time of Anodes for Lithium-Ion Batteries through Simultaneous Multilayer Coating. *Energy Technol.* **2021**, *10*, 2100367. [CrossRef]
9.   Jaiser, S.; Müller, M.; Baunach, M.; Bauer, W.; Scharfer, P.; Schabel, W. Investigation of film solidification and binder migration during drying of Li-Ion battery anodes. *J. Power Sources* **2016**, *318*, 210–219. [CrossRef]
10.   Börner, M.; Friesen, A.; Grützke, M.; Stenzel, Y.P.; Brunklaus, G.; Haetge, J.; Nowak, S.; Schappacher, F.M.; Winter, M. Correlation of aging and thermal stability of commercial 18650-type lithium ion batteries. *J. Power Sources* **2017**, *342*, 382–392. [CrossRef]